# Temporal and spatial reflectivity of focused beams in stimulated Brillouin scattering for phase conjugation

Ralf Menzel and Hans J. Eichler
*Optisches Institut, Technische Universität Berlin, Strasse des 17, Juni 135, 1000 Berlin 12, Germany*
(Received 22 November 1991; revised manuscript received 29 July 1992)

The buildup and decay of the sound-wave gratings in stimulated-Brillouin-scattering cells were calculated taking into account the spatial dependence in the propagation direction of the focused laser beams. The incident intensities were varied up to the saturation values. The influence of the different parameters such as focal length, cell length, pulse duration, and phonon lifetime is discussed.

PACS number(s): 42.65.Hw, 42.65.Es

## I. INTRODUCTION

Stimulated Brillouin scattering (SBS) of laser radiation in liquids or gases is progressively applied for building phase-conjugating mirrors in laser systems [1–27]. These self-pumped mirrors are simple and handy devices for designing double and multipass amplifiers (MOPA's) (e.g., [3–16]) or oscillators [17–27] if the incident intensities (or powers, respectively) are high enough to provide sufficient reflectivity from the SBS process. The phase-conjugating properties of these mirrors were successfully used for compensating phase distortions in high-power laser systems, especially the thermal lens of strongly pumped solid-state laser rods. They are also useful for high-quality beam combining after separate amplification [28–31] or for $Q$ switching [24–27]. Techniques for pulse compression [32], picosecond-pulse generation [33], and reflection of ps pulses [34] based on SBS have also been described.

The reflectivities of SBS mirrors depend on the excitation conditions and the material properties. Several approaches for calculating the scattering process were discussed [35–42]. The basic equations have been given in several forms [35–39]. But the complete solution of these coupled partial differential equations for the incident and reflected light waves and the sound-wave grating requires a great numerical effort and has not been done yet. Different approximations were therefore investigated. Especially, the steady-state case was explored in detail (e.g., [39,42]). A universal formula for the reflectivity as a function of the incident light power and the threshold value of the material was given under these assumptions [42].

A self-pumped SBS mirror often simply consists of a lens focusing the incident beam into the nonlinear material. Frequently it is assumed that the reflecting sound wave builds up near the focus of the lens. If a Gaussian laser beam is incident one could expect the sound wave to have a longitudinal extension of about the confocal parameter of the Rayleigh length of the beam. However, detailed calculations relating the distribution of the incident focused beam power and the extension of the sound wave produced by stimulated scattering are not available.

The extension of the sound wave is especially important when laser fields with large bandwidth and small coherence length are applied. To obtain low SBS threshold and high reflectivity in this case, the coherence length should exceed the longitudinal sound-wave extension [43–47] so that an efficient coherent wave interaction is possible. (Although the SBS process has no threshold of the reflectivity as a function of the incident light power or energy which will define exactly the reflection onset, a strong increase of many orders of magnitude of the reflectivity takes place in a very small power or energy range of a few percent. Therefore a threshold power or energy may be defined above which reflectivities larger than, e.g., 2% are obtained [39].)

For designing laser systems with SBS mirrors a detailed knowledge of the buildup and decay of the sound-wave grating in the SBS medium and thus the temporal and spatial distribution of the induced reflectivity is essential. The quality and fidelity of the phase conjugation depend strongly on these details as investigated, e.g., in Refs. [48–51].

Only in cases where the reflection takes place in a sufficiently small area are the phases of different parts of the scattered beam expected to be correlated resulting in perfect phase conjugation. Otherwise, piston errors may occur between these parts and therefore no accurate reconstruction of the original signal takes place. In this case large statistical fluctuations were observed in the fidelity [51], especially at high input powers. On the other side, the power (energy) has to be well above the "threshold" of the nonlinear reflectivity curve. Otherwise the fidelity of the reflected signal becomes small, because the wing parts of the incident (Gaussian) beam with energies below this threshold value are not reflected [51]. A decrease of the diameter then could be observable in the phase-conjugated beam.

The useful power (energy) range of the incident radiation is limited by the SBS threshold at the lower limit and by optical breakdown (OBD) at maximum values (e.g., [42]). Therefore choice of optimal focusing lenses for applications should be done considering the distribution of the reflectivity in the focal range in the medium as a function of the applied pulse energy at a given pulse length.

In the same manner the influence of the length of the

 

SBS cells used will be discussed. The situation in the medium appears different if the whole range between the lens and the beam waist is filled with the SBS medium or if the SBS medium covers only a small length around the Rayleigh range. Further, the change of the reflectivity as a function of the pulse duration has to be considered.

For a better understanding of the influence of the experimental parameters discussed, the development of the amplitude, and thus the reflectivity, of the sound-wave grating is computed here under conditions used for practical applications. This allows a theoretical discussion of the influence of the different parameters such as the focal length of the lenses used, the length of the SBS cells, the duration of the laser pulses used, and the choice of the applied material.

## II. MODEL

Our system of coupled differential equations is based on approximations described in Refs. [36,39]. The description of the incident and reflected light waves and their coupling with the sound wave is simplified by the assumptions of slowly varying amplitudes (SVA) of the electric fields and the acoustic wave. This condition is well fulfilled for the light waves but the pump pulse duration (e.g., 20 ns) is only five times longer than the period of the sound wave (e.g., 4 ns) in practical cases. Nevertheless, it is assumed that the SVA approximation gives at least qualitatively good results. In addition the influence of the pump frequency bandwidth or coherence time should be discussed [36] if the calculations are compared with experiments. The exact transversal shape of the light is neglected in the differential equations but the intensity variation along the beam axis due to the focusing is considered.

The differential equations for the electric fields, as given in [36], can be transformed to equations for the intensities of the light beams using the following further approximations [39]. The frequencies of the pump and reflected light are set equal and phase locking between the pump wave, the reflected (Stokes) wave, and the sound wave is assumed. This phase locking will be fulfilled for monochromatic light by the nonlinear properties of the SBS process itself, because of the much higher gain coefficient of light with the right phase compared to a statistical phase. If broadband light were used, phase locking would be expected only within the coherence length and the following theoretical description would also be restricted to this region. Further, negligible absorption of the light in the SBS medium is assumed in agreement with the practical case.

Using these assumptions the process of buildup and decay of the sound-wave grating amplitude $S$ by the incident intensity $I_{\text{inc}}$ and the intensity of the reflected light $I_{\text{out}}$ is described by

$$\frac{\partial I_{\text{inc}}(z,t)}{\partial z} = -S(z,t)[I_{\text{inc}}(z,t)I_{\text{out}}(z,t)]^{1/2} , \tag{1}$$

$$\frac{\partial I_{\text{out}}(z,t)}{\partial z} = -S(z,t)[I_{\text{inc}}(z,t)I_{\text{out}}(z,t)]^{1/2} , \tag{2}$$

$$\frac{\partial S(z,t)}{\partial t} = \frac{1}{2\tau_B}\{g[I_{\text{inc}}(z,t)I_{\text{out}}(z,t)]^{1/2} - [S(z,t) - S_0]\} , \tag{3}$$

with $g$ denoting the stationary Brillouin gain, $\tau_B$ the phonon lifetime, and $S_0$ the initial (spontaneous) sound-wave amplitude. The gain may be calculated from the light frequency $\omega$, the electrostrictive coefficient $\gamma_e$, the velocities of light and sound $c$ and $v$, the refractive index $n$, the density $\rho_0$, of the material:

$$g = \frac{\omega^2 \gamma_e^2 \tau_B}{c^3 v n \rho_0} . \tag{4}$$

The focusing and the resulting change in the intensity of the pump and SBS light will be approximately considered in the following way (see Fig. 1). If Gaussian beams are assumed, the radius ($1/e^2$ value for the intensity) of the focused light $w(z)$ is given by the following function of the coordinate $z$ (see Fig. 1):

$$w(z) = \left[ \frac{w_0^4 \pi^2 + (z - z_0)^2 \lambda^2}{w_0^2 \pi^2} \right]^{1/2} , \tag{5}$$

where $w_0$ is the waist radius of the Gaussian beam at the position $z_0$ and $\lambda$ the light wavelength. The beam area $A(z)$ is then obtained as

$$A(z) = \frac{w_0^4 \pi^2 + (z - z_0)^2 \lambda^2}{w_0^2 \pi} . \tag{6}$$

The intensities of the incident and reflected light beams are assumed to vary by this changing area in addition to the interaction with the SBS material. The differential quotients in Eqs. (1) and (2) have therefore to be completed by

$$\frac{\partial I_{\text{inc(out)}}(z,t)}{\partial z} \rightarrow \frac{\partial I_{\text{inc(out)}}(z,t)}{\partial z} + \frac{I_{\text{inc(out)}}(z,t)}{A(z)} \frac{\partial A(z)}{\partial z} . \tag{7}$$

Introducing the power $P_{\text{inc(out)}}(z,t) = I_{\text{inc(out)}}(z,t) A(z)$ the system of partial differential equations (1)–(3) then can be written as

$$\frac{\partial P_{\text{inc}}(z,t)}{\partial z} = -S(z,t)[P_{\text{inc}}(z,t)P_{\text{out}}(z,t)]^{1/2} , \tag{8}$$

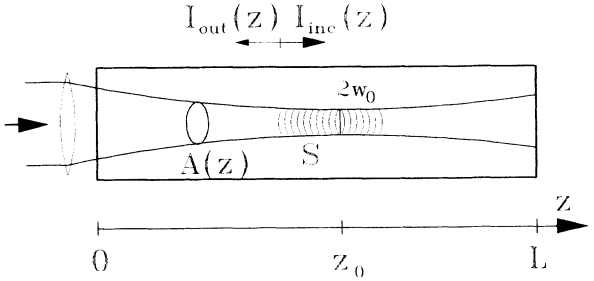


FIG. 1. Intensities $I_{\text{inc}}$ and $I_{\text{out}}$ and beam area $A$ are functions of the longitudinal coordinate $z$.

$$\frac{\partial P_{\text{out}}(z,t)}{\partial z} = -S(z,t)[P_{\text{inc}}(z,t)P_{\text{out}}(z,t)]^{1/2} , \quad (9)$$

$$\frac{\partial S(z,t)}{\partial t} = \frac{1}{2\tau_B}\left\{ g\frac{[P_{\text{inc}}(z,t)P_{\text{out}}(z,t)]^{1/2}}{A(z)} - [S(z,t)-S_0]\right\} . \quad (10)$$

The variation of the area does not affect Eqs. (1) and (2) if the power of the light beams is used. The additional differential quotient of $A(z)$ in Eq. (7) is compensated by a term resulting from the substitution of the intensities by the powers so that Eqs. (8) and (9) have the same form as Eqs. (1) and (2). However, Eq. (3) changes into Eq. (10) describing the focusing of the incident beam.

The initial scattering of the incident light is considered by the spontaneous sound-wave amplitude $S_0$. It describes the phonon fluctuations in the medium, but may also contain other kinds of appropriate scattering for starting the SBS process. As will be shown later, the size of $S_0$ determines the threshold of the SBS process and is used to fit the numerical calculations to the experimental results.

## III. NUMERICAL SOLUTION

The system of differential equations (8)–(10) was solved numerically with a simple Euler method combined with a self-consistent iteration procedure for the beam powers.

### A. Numerical procedure

The powers $P_{\text{inc(out)}}(z,t)$ (and intensities) were calculated for the given amplitudes of the sound-wave grating $S(z,t_n)$ at each time step $n$ by a self-consistent iteration of their distribution in space starting from the noise level. This iteration was stopped as soon as the power of the reflected light did not change more than a given limit. The variation of the amplitude of the sound-wave grating from the $n$th to the $(n+1)$st time step was calculated using the calculated light power distribution of the $n$th step. With this procedure the transfer of possible numerical errors in the calculated light powers from time step to time step, caused by the limited accuracy of the computer, could be excluded. The use of the results for the powers from the $n$th step as starting value for the iteration of the $(n+1)$st step was not investigated systematically. In the cases checked the computing time could be reduced by a factor 2 and the deviation of the results was very small.

First trials using more sophisticated routines for solving the system of partial differential equations did not improve the quality of the calculation significantly, but increased the computation time. This may result from the nonlocal influence of the light powers. The power decrease of, e.g., the incident light at the front of the cell is dependent on the power of the reflected light at the same position. But this power is the result of the summation of all contributions to the reflection over the whole cell. Therefore sufficient numbers of space steps and iterations were necessary.

### B. Step widths and accuracy

The correct choice of the step widths in space and time was checked by considering the stability of the calculated values of the reflectivities and the maximum amplitude and position of the sound wave. The stability of the pulse energy reflectivity and the maximum amplitude of the sound wave was better than $10^{-3}$ if 3000 space steps were used and the truncation value was less than $10^{-4}$. The same accuracy was reached in the temporal evolution if 1000 time steps or more were used. Further decrease of the truncation value down to $10^{-6}$ improved the stability up to $10^{-5}$ and doubled the computation time, roughly. As sufficient compromise we used 3000 spatial steps and 1000 time steps in combination with a truncation value of $10^{-4}$ for all calculations. For plotting the data, only 50 time intervals and 200 space intervals were used to keep the size of the three-dimensional representations readable.

### C. Computing time

The program was implemented in QUICKBASIC4.5 with double-accuracy floating-point number calculation and used in the compiled version. In most cases about 8–12 iterations of the intensity calculation were needed in each time step. Using a personal computer with 486 processor (including a math coprocessor) running at 33 MHz it takes about 1 s for each of these iterations over 3.000 space steps. The overall computing time for one complete solution in time and space is therefore on the order of 4 h on this type of computer.

### D. Experimental parameters

As mentioned above, the calculated results can be fitted to experimental data by choosing the appropriate spontaneous sound-wave amplitude $S_0$, describing the spontaneous reflectivity. Its influence on the shape of the reflection curve as a function of the energy will be described in detail in Sec. IV D.

For calibration of the model the experimental threshold energy of 6.9 mJ in $SF_6$ at 20 bars as given in [52] was used. The experimental cell length was 6.4 cm and the half-width [full width at half maximum (FWHM)] of the pump pulse 10 ns. It is pointed out that the measured threshold energy is much below the value given in [39]. This may be due to the good coherence and beam profile of the laser used in [52].

The material parameters were chosen as $g=0.014$ cm/MW for the gain and $\tau_B=17$ ns for the phonon lifetime. The phonon lifetime was calculated for the wavelength $\lambda$ of the Nd:YAG (neodymium-doped yttrium aluminum garnet) laser of 1064 nm based on the results given in [53] and the gain was taken from this reference, too. The best fit was obtained with $S_0=2\times10^{-4}$ cm$^{-1}$ which has therefore been used in all further calculations.

The $S_0$ value of $2\times10^{-4}$ cm$^{-1}$ resulted in the calculations in an initial energy or power or intensity reflectivity of $10^{-6}$ for a cell of $L=10$ cm length. This result can be checked by the analytical integration of Eq. (9) under the assumption of constant $P_{\text{inc}}$ and $S_0$. From

$$\int_0^{P_{\text{out.0}}} \frac{1}{[P(t)_{\text{out}}]^{1/2}} dP_{\text{out}} = \int_L^0 -S_0[P(t)_{\text{inc}}]^{1/2} dz \qquad (11)$$

follows

$$R = \frac{P(t)_{\text{out.0}}}{P(t)_{\text{inc}}} = \tfrac{1}{4} S_0^2 L^2 \ . \qquad (12)$$

This equation leads exactly to the numerically calculated initial scattering reflectivity of $R = 10^{-6}$ for $L = 10$ cm and confirms so far the quality of the computation. This initial reflectivity should be distinguished from the reflectivity of the spontaneous Brillouin scattering, which is caused by an incoherent sound wave propagating in the $z$ direction. In contrast, $S_0$ describes the amplitude of a harmonic sound wave which reflects the incident wave coherently. This well-defined sound wave is represented by a suitable Fourier component of the incoherent ultrasound distribution thermally excited in the SBS medium.

The initial sound-wave amplitude $S_0$ is expected to be a function of the focusing conditions and cell length $L$. However, in the following computations $S_0$ was set constant as a first approach. In most practical cases the general features of the temporal and spatial reflectivity distribution will be affected only weakly by this approximation, e.g., the threshold energy depends only on the logarithm of $S_0$ (see Sec. IV D).

## IV. RESULTS AND DISCUSSION

For discussion of the influence of the different parameters on the temporal and spatial distribution of the two light waves and the sound-wave grating a standard set of values will be used.

### A. Standard parameter set

The energy of the pump pulse with a Gaussian temporal and spatial shape at a wavelength of 1064 nm was chosen to be 25 mJ and its half-width (FWHM) to be 20 ns resulting in a maximum power of 1.2 MW. The beam of 3 mm diameter was assumed to be focused with a lens of 10 cm focal length into a cell of 10 cm length with a waist position at 9.5 cm. The beam waist diameter for these focusing conditions was about 0.04 mm and the Rayleigh length 1 mm. The material parameters of $SF_6$ were used as given above. The spontaneous scattering $S_0$ was set to $2 \times 10^{-4}$ cm$^{-1}$. These parameters were used in all calculations if not stated differently.

### B. Light and sound distribution in time and space

The numerical solution of Eqs. (9)–(11) allows the visualization of the buildup and decay of the sound-wave grating, the depletion of the incident pump intensity and power, and the development of the power of the reflected light as functions of the position in the cuvette. In Figs. 2–5 these results are shown for the standard set of parameters.

Figure 2 shows the focusing of the incident light intensity which is localized around the beam waist at 9.5 cm.

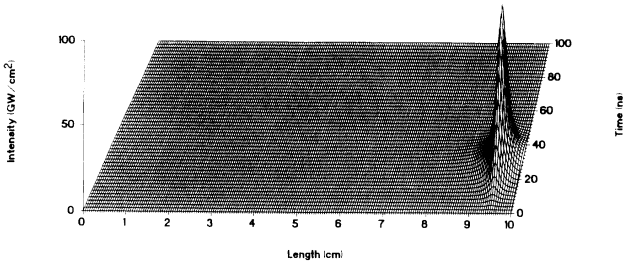


FIG. 2. Spatial and temporal intensity distribution of the incident light pulse of 25 mJ with 20-ns half-width peaking at 30 ns and focused with a 100-mm lens; standard conditions.

This intensity distribution may be compared with the distribution of the sound-wave grating in Fig. 5.

The spatial distribution of the incident power versus time is shown in Fig. 3. The depletion of the incident light starts at about 23 ns, i.e., before the maximum of the pulse at 30 ns. At later times the incident light is weakened even at the front end of the cell within the first 3 cm. In Fig. 4 the complementary power distribution of the reflected light is shown. Reflection becomes considerable about 8 to 6 ns before the peak of the pump pulse and about 2 mm in front of its waist.

This behavior becomes understandable from Fig. 5, which shows the development of the amplitude of the sound-wave grating for the same experimental conditions as all other pictures of Fig. 2.

The maximum of the sound amplitude is located about 1.5 mm in front of the beam waist of the focused light. Almost no sound wave is excited behind the beam waist at 9.5 cm. This result was obtained even with very gentle focusing (see Fig. 20) where the sound wave and the power of the reflected light are also almost zero behind the beam waist. This effect may be understood as a consequence of the very high nonlinearity of the SBS process. The power of the reflected light changes typically over six orders of magnitude from the noise level up to the magnitude of the pump power.

Another unexpected result is the wide distribution of the sound wave over a large part of the cell, even at the applied pump energy of 25 mJ only three times above threshold. The sound wave has an extension of more than 1 cm whereas the Rayleigh length of the focused laser beam amounts to only 1 mm.

Nevertheless, the first buildup of the sound-wave amplitude is concentrated in the focal region of the incident

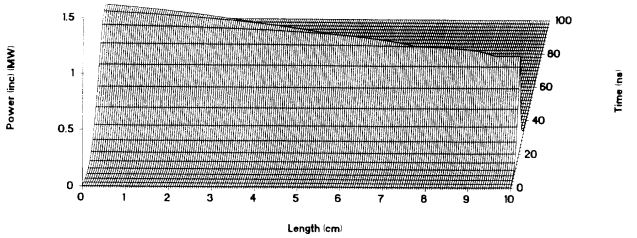


FIG. 3. Power of the incident light pulse; conditions as in Fig. 2.

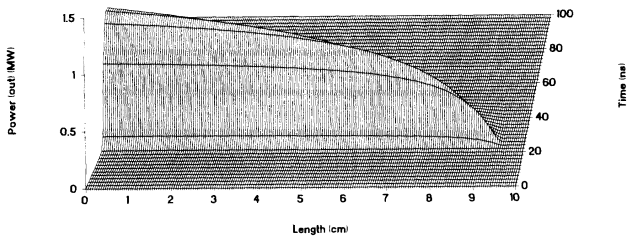


FIG. 4. Power of the reflected light; conditions as in Fig. 2.

beam. Therefore the characteristic interaction length $L_{\text{threshold}}$ determining the product $gI_{\text{threshold}}L_{\text{threshold}}$ at the threshold of the SBS will be in the range of the Rayleigh length. Choosing, e.g., $L_{\text{threshold}}=0.8$ mm, which is slightly smaller than the Rayleigh length of 1 mm, leads to the commonly used product $gI_{\text{threshold}}L_{\text{threshold}}=30$ [54] for our standard parameters. The computed sound-wave distribution showed such widths at the very beginning. It should be noted, however, that the $gI_{\text{threshold}}L_{\text{threshold}}$ product is derived for the description of stationary SBS whereas transient scattering is treated here.

### C. Influence of the pump energy

The energy reflectivity increases with the energy of the incident light pulse (see Figs. 10, 12, and 15). The temporal reflectivity changes too, because of the changing input power and the time constant of the sound wave. With increasing pulse energy the temporal shape of the reflected pulse (see Fig. 6) approaches more and more the shape of the incident pulse. But even at very high powers an initial delay of the reflectivity can be observed. This delay appears as one of the reasons for energy reflectivities below 100%.

This behavior becomes more obvious if the temporal reflectivity as the ratio of the incident and the reflected power as a function of time is plotted (see Fig. 7). The pump energy also influences the distribution of the sound-wave grating. In Figs. 8 and 9 examples are given for excitation energies of 8 and 100 mJ.

At low energies the sound wave is delayed with respect to the incident light pulse. The spatial distribution at low energies is more concentrated in a range close to the focus of the pump beam. The effective length can be obtained in the mm range.

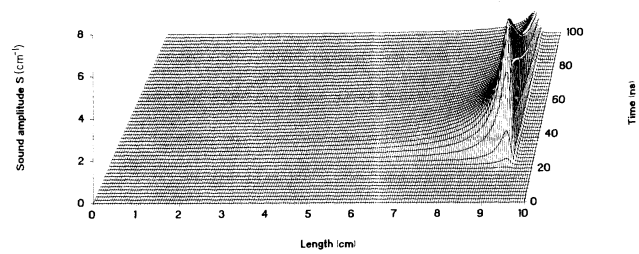


FIG. 5. Amplitude of the sound-wave grating; conditions as in Fig. 2.

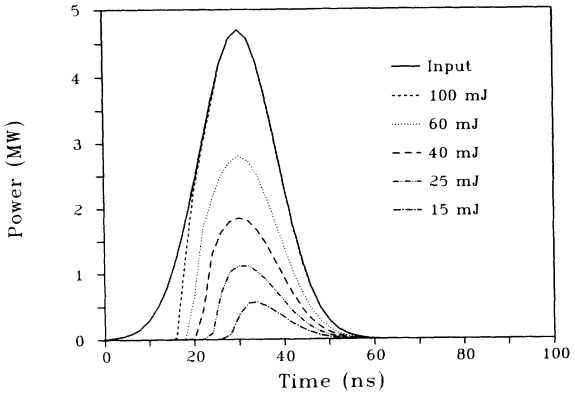


FIG. 6. Powers of the incident and the reflected light as functions of time at the position of the entrance window of the cell ($z=0$); besides the given energies standard parameters were used.

If the energy is enlarged the sound wave will appear earlier in both time and space. High excitation energies can lead to a remarkable amplitude in the first part of the cell (see Fig. 9). Nevertheless, the sound wave always appears first near to the waist of the beam. In the case of very high excitation energies the sound-wave maximum can move back and forth to the waist region for long times. Of course, it decays everywhere according to the phonon lifetime (17 ns in the examples shown).

### D. Influence of the spontaneous sound-wave amplitude $S_0$

The spontaneous sound-wave amplitude $S_0$ determines the threshold energy of the reflectivity (Fig. 10).

The most obvious difference of the calculated curves with $S_0$ values of $2\times10^{-3}$, $2\times10^{-4}$ $2\times10^{-5}$, and $2\times10^{-6}$ cm$^{-1}$ is the change in the threshold energies $E_{\text{th}}$. Therefore the threshold energies were plotted in a semilogarithmic scale versus the spontaneous sound-wave

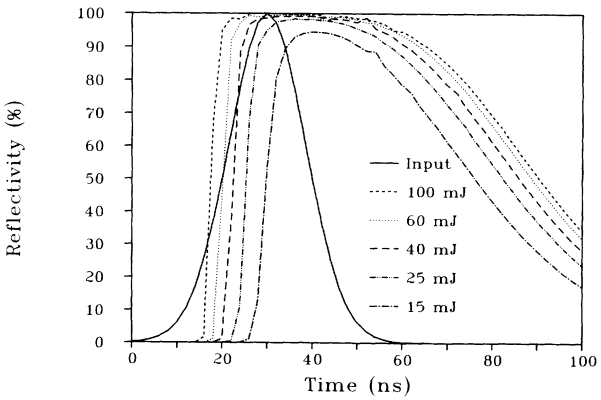


FIG. 7. Temporal reflectivity as a function of time at the position of the entrance window of the cell ($z=0$); solid line marks the time profile of the incident light pulse; besides the given energies the standard parameters were used.

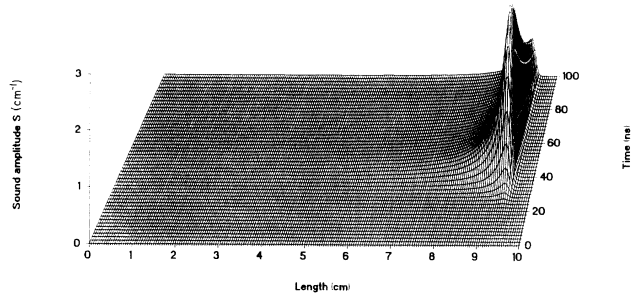


FIG. 8. Distribution of the sound wave in time and space for the excitation of 8 mJ and standard conditions otherwise.

amplitude $S_0$ (see Fig. 11).

The linear regression gives an excellent correlation. If the curves of Fig. 10 are normalized for the threshold energy they show almost the same shape within the computation error. Therefore, within the usual measuring error the shape of the normalized energy reflection curves, as functions of the energies may be assumed to be nearly independent of $S_0$. A similar behavior was proposed in Ref. [42] for the stationary solution with no focusing of the beams.

### E. Influence of the phonon lifetime $\tau_B$

As an important material property the influence of the phonon lifetime on the reflection of the SBS cell will be discussed. In liquids this decay time is smaller than in gases by more than one order of magnitude. Therefore the case of a ten times smaller phonon lifetime was investigated. According to Eqs. (3) and (4) the gain should be reduced by a factor of 10, also, to keep $g/\tau_B$ constant. The result of the computation is shown in Fig. 12.

Reduced phonon lifetime results in an increase of the threshold energy and a reduced slope of the energy reflectivity as a function of the incident pulse energy. However, the shape of the reflectivity curve for the two different phonon lifetimes is very similar. To demonstrate the similarity the reflectivity is given also for $\tau_B = 1.7$ ns and $g = 0.003$ cm/MW. The change of the gain coefficient corresponds only to a power scaling and reduces the threshold within the ratio of the gain coefficients.

The curves with $\tau_B = 17$ ns and $g = 0.014$ cm/MW and $\tau_B = 1.7$ ns and $g = 0.003$ cm/MW should be compared to estimate the influence of the phonon lifetime on the

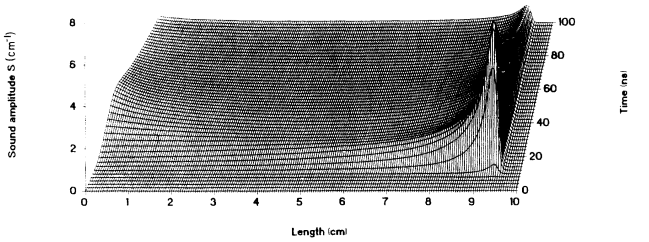


FIG. 9. Distribution of the sound wave in time and space for the excitation of 100 mJ and standard conditions otherwise.

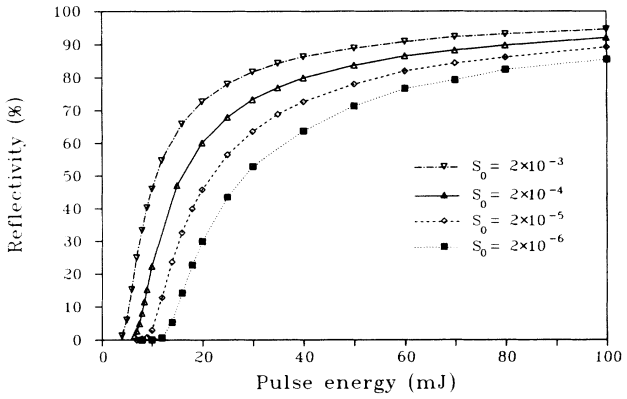


FIG. 10. Energy reflectivity as a function of the energy of the incident light pulse calculated with the standard parameters but different $S_0$.

slope of the reflectivity curve. Some small influence of the phonon lifetime on the reflectivity curve is evident whereas a change of the gain coefficient does not affect the shape of this curve, if they are normalized for the same threshold energy (see Sec. IV F).

In Figs. 13 and 14 the time dependencies of the reflected power and the temporal reflectivities are shown for the artificial material with a phonon lifetime of 1.7 ns and a gain of 0.0014 cm/MW.

Figure 13 should be compared to Fig. 6. Again a delay of the reflected pulse can be observed but the trailing part of the reflected pulse does not approach the incident pulse as much as in Fig. 6. Although the phonon lifetime is smaller than $\frac{1}{10}$ of the pulse width this nonstationary behavior is observable in Fig. 14. This result may be due to the high nonlinearity of the SBS process again. The decay of the sound wave has to be evaluated by comparing the SBS with the share of the spontaneous reflected light, which may be six orders of magnitude smaller. The corresponding temporal reflectivity is shown in Fig. 14.

The spatial and temporal distribution of the sound wave is given in Fig. 15 for the artificial material with a phonon lifetime of 1.7 ns, a gain of 0.0014 cm/MW, and

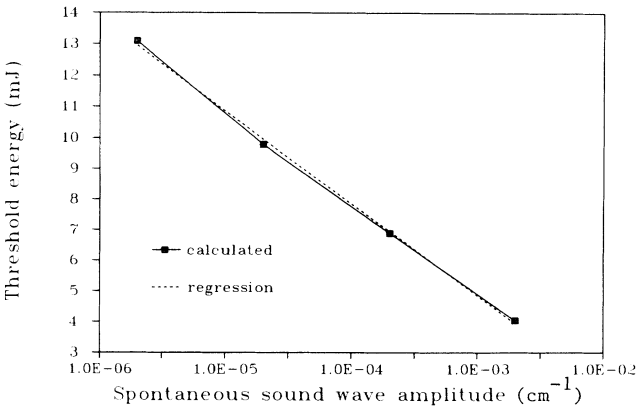


FIG. 11. Threshold energies from Fig. 11 vs the spontaneous scattering $S_0$.

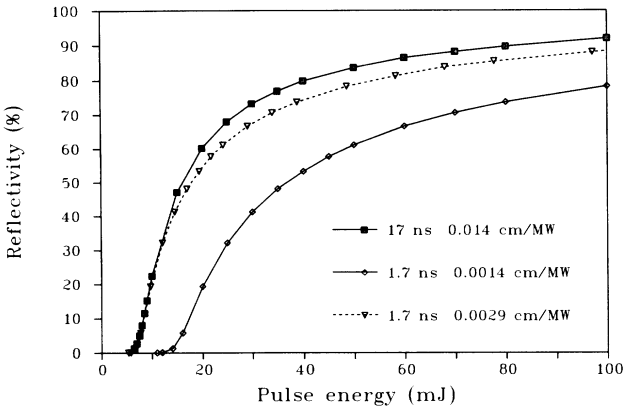


FIG. 12. Energy reflectivity as a function of the energy of the incident light pulse calculated with the standard parameters and for different phonon lifetimes and gain values.

an excitation energy of 25 mJ for comparison with Fig. 5.

As can be seen, the sound wave decays almost completely within the duration of the pump pulse but the spatial distribution is quite comparable to the case of Fig. 5.

### F. Influence of the gain $g$

As can be seen from Eqs. (8)–(10) the gain $g$ occurs in the product with the powers $P_{inc}$ and $P_{out}$ only. Therefore a change in the gain is exactly equivalent with a rescaling of the powers. The result for the energy reflectivity as a function of the pump energy for the standard conditions but different gains is depicted in Fig. 16.

All these curves are identical if normalized to the same threshold energy or power. Therefore materials with lower gain show a higher threshold and a slower increase of the reflectivity with increased pumping. The saturation demands much higher pump energies.

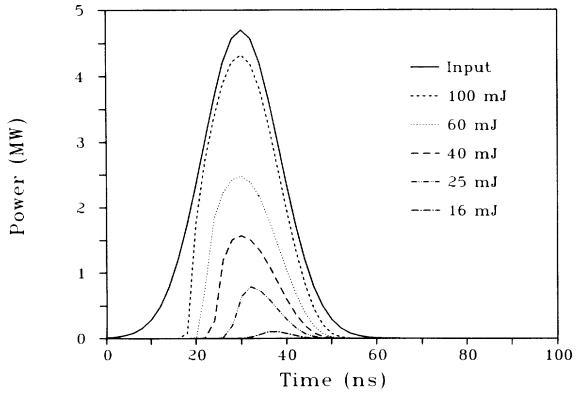


FIG. 13. Powers of the incident and the reflected light as functions of time at the position of the entrance window of the cuvette ($z=0$); besides the given energies, a phonon lifetime of 1.7 ns, and a gain of 0.0014 cm/MW, the standard parameters were used.

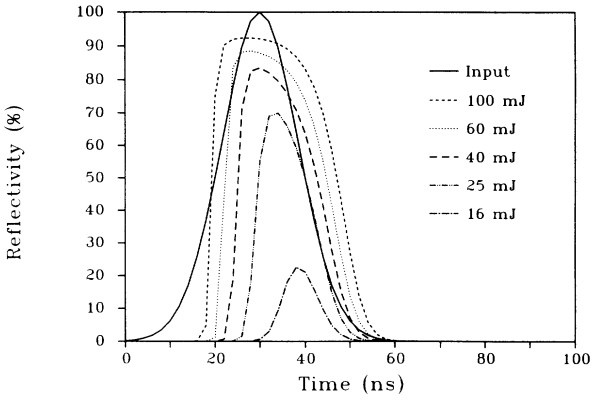


FIG. 14. Temporal reflectivity as a function of time at the position of the entrance window of the cuvette ($z=0$); solid line marks the time profile of the incident light pulse; besides the given energies, a phonon lifetime of 1.7 ns, and a gain of 0.0014 cm/MW, the standard parameters were used.

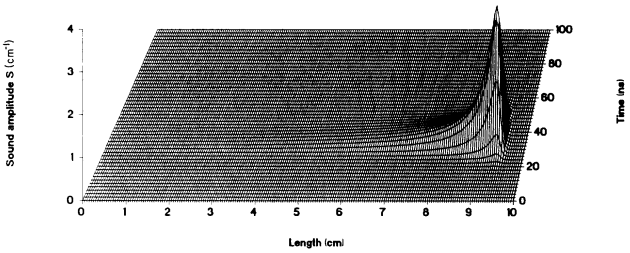


FIG. 15. Distribution of the sound wave in time and space for the standard condition but a phonon lifetime of 17 ns, a gain of 0.0014 cm/MW, and an excitation energy of 25 mJ (compare with Fig. 5).

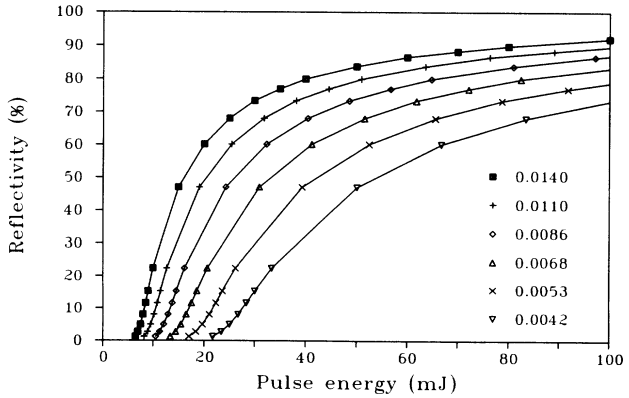


FIG. 16. Energy reflectivity as a function of the energy of the incident light pulse calculated with the standard parameters but different gains $g$ (values in cm/MW).

### G. Reflectivity as a function of the pulse width

In Fig. 17 the energy reflectivity as a function of the pulse half-width (FWHM) for pump pulses with a fixed peak power of 1.2 MW and therefore variable energy or a fixed energy of 25 mJ and thus variable power, respectively is shown.

As could be expected from the discussion of the influence of the phonon lifetime the increase of the pulse width coupled with a proportional increase of the excitation energy will increase the reflectivity to values above 90%. On the other side, short pulses of the same peak power are below threshold, e.g., the 2-ns pulse in Fig. 17.

If pump pulses of constant energy (of, e.g., 25 mJ as in Fig. 18) are used the reflectivity is almost constant over a range of variable pulse widths (from 0.6 to 10 ns in the example). For pulse widths larger than the phonon lifetime a decrease of the reflectivity occurs. In the given example of Fig. 17 pump pulses of 25 mJ and 600 ns half-width do not reach the SBS threshold.

An example for the distribution of the sound wave excited by a short pump pulse of 25 mJ and 6 ns width is given in Fig. 18.

Although our SVA calculation does not fulfill the condition of a short sound-wave period (4 ns for $SF_6$) compared to the pulse width, the qualitative result seems to be correct. The sound wave decays with the phonon lifetime of 17 ns which is larger than the incident pulse width in this case. The spatial shape of the distribution is quite similar to the standard case as shown in Fig. 5.

### H. Reflectivity as a function of the focal length

The focal length of the lens used can be changed easily when setting up SBS experiments. For laser systems using a SBS cell as phase-conjugating mirror the focal length can be optimized for best reflectivity and reliability. Some results of our model on the influence of the focal length on the SBS process are shown in Figs. 19 and 20.

In a first approximation a decrease of the Rayleigh length should be compensated by an increasing intensity

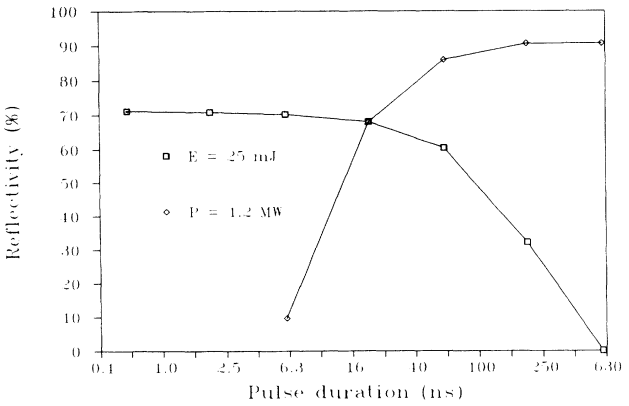


FIG. 17. Energy reflectivity as a function of the pulse width for pump pulses with a fixed peak power of 1.2 MW or a fixed energy of 25 mJ; all other parameters are the standard set.

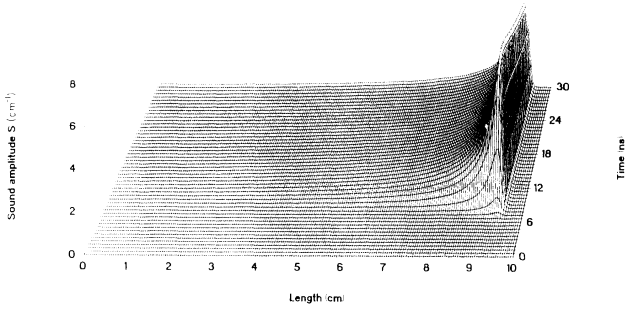


FIG. 18. Distribution of the sound wave in time and space for excitation with 25 mJ, pulse width of 6 ns, and standard conditions otherwise (Compare Fig. 5).

(decreasing area) and therefore the reflectivity should remain constant as a function of the focal length. Within a variation of 4% this result could be confirmed by the calculations with a constant $S_0$. For the comparison of these results with experimental data the coherence length of the laser used, the influence of the cell length (see Sec. IV I), and the possible variation of $S_0$ (see Sec. III D) have to be considered. The distribution of the sound wave is shown for two focal lengths of 5 and 200 cm in Figs. 19 and 20 in addition to the result for the focal length of 10 cm in Fig. 5.

In the case of strong focusing the sound wave is localized strongly in the waist region. It starts very steeply in front of the waist position and reaches its maximum in time at about the peak of the pump pulse. The sound amplitude at the cell front can be neglected.

The sound-wave distribution in Fig. 20 representing the use of a 200-cm lens appears completely different from Fig. 19, although the energy reflectivities of 72% and 68% for the two focal lengths 5 and 200 cm are very close. The sound wave in Fig. 20 is distributed over the whole cuvette and the amplitude is about two orders of magnitude smaller.

The results of these calculations can be used for the optimization of the focal length. Choosing short focal lengths will lead to very compact sound-wave distributions with the advantage of low demands on the coherence of the laser light and probably good phase-conjugating properties. Because of this small distribution

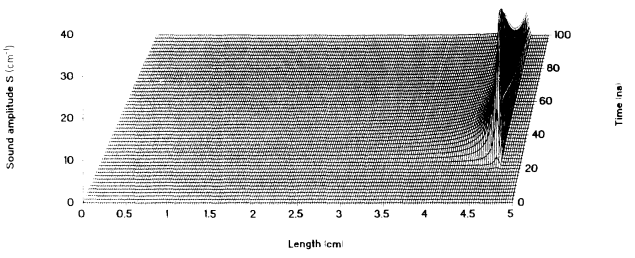


FIG. 19. Distribution of the sound wave in time and space for focusing with an $f = 50$ mm lens and a waist position 47.5 mm behind the cuvette entrance window; standard conditions otherwise.

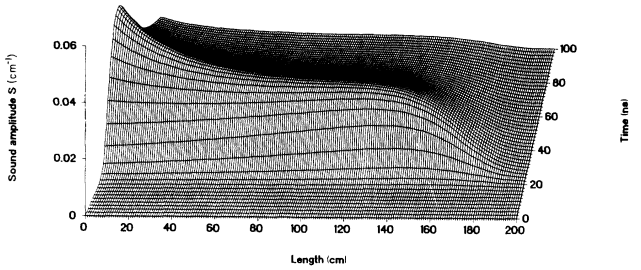


FIG. 20. Distribution of the sound wave in time and space for focusing with an $f=200$ mm lens and a waist position 190 mm behind the cell entrance window; standard conditions otherwise.

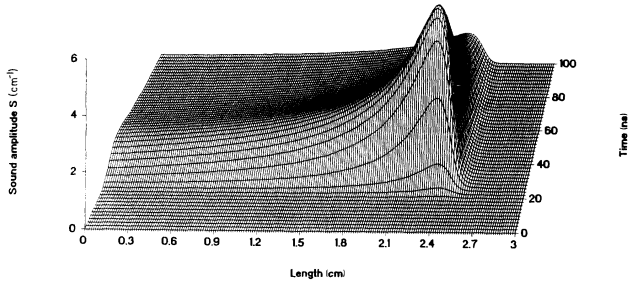


FIG. 22. Distribution of the sound wave in time and space for a waist position 2.5 cm behind the cell entrance window (standard conditions otherwise).

piston errors may be minimized. The main disadvantage of very short focal lengths is the high intensities and therefore the occurrence of optical break down. Thus the focal lengths should be optimized for both effects for a given power and energy of the pump pulse. In certain cases no really satisfying focal length may be possible. In these cases an oscillator amplifier configuration with two SBS cells may be adequate [40].

### I. Reflectivity as a function of the length of the cuvette

As mentioned above, the length of the cuvette used and the corresponding distance of the beam waist from the entrance window of the cuvette may influence the energy reflectivity and even more the distribution of the sound wave in the cell. In Fig. 21 the results of calculations with variable cell lengths are shown. As long as this length is not too short compared to the Rayleigh range of the focused beams the reflectivity increases quite slowly with cell length. For very short lengths a decrease of reflectivity of more than 5% occurs. This decrease is explained by different distributions of the sound waves for the different lengths. In Figs. 22 and 23 the sound-wave distribution for beam waist positions 25 and 0.625 mm behind the cell window are shown.

Again it can be seen clearly that the sound wave is built in front of the waist position. In Fig. 23 the amplitude of the sound wave has its maximum at the position of the cell entrance. Compared to the situation in Fig. 5 a stronger sound wave occurs in the first part of the cell in both Figs. 22 and 23. This result should be considered in addition to the limited damage threshold of the entrance window of the SBS cells in choosing the right position of the beam waist in the cell. In general it seems reasonable to set the waist as far as possible from the cell entrance window.

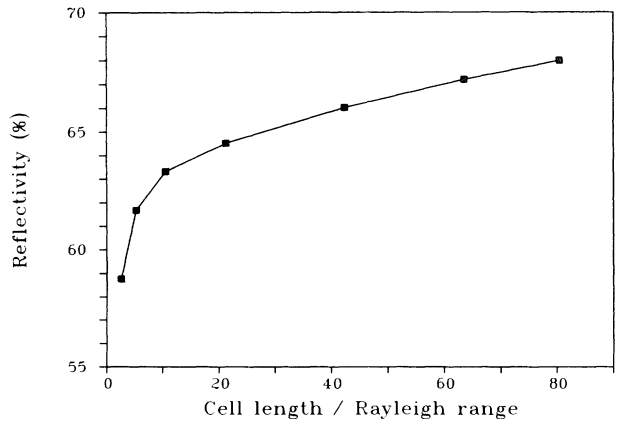


FIG. 21. Energy reflectivity as a function of the cell length in front of the beam waist (standard conditions otherwise).

## V. CONCLUSIONS

To calculate the axial distributions of the sound and light in the SBS cells we started from a plane-wave equation extended to include the peak intensity variation of the Gaussian beam due to focusing. Of course, our one-dimensional approximations should be checked by two- or three-dimensional calculations. However, our approach already indicated some interesting features of SBS by focused laser beams:

(1) Depending on the focal length of the entrance lens the sound wave may be sharply concentrated in the cell or distributed over the whole cell length.

(2) The sound-wave extension may considerably exceed the Rayleigh length of the incident laser beam.

(3) The sound wave is built up mainly in front of the incident beam waist.

(4) At higher incident intensities the sound wave is first built up near to the beam waist but may later have its maximum at the front of the SBS cell. Further oscillation of the sound maximum back to the beam waist is possible.

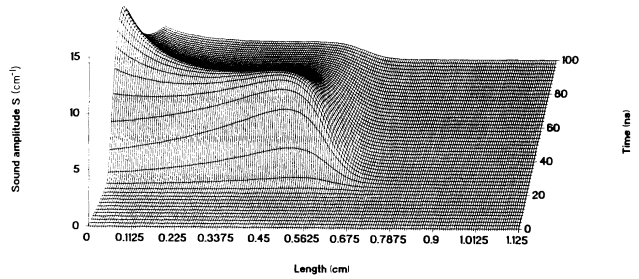


FIG. 23. Distribution of the sound wave in time and space for a waist position 0.625 mm behind the cell entrance window (standard conditions otherwise).

The given model and the calculated results may be used for a more detailed understanding of the influences of the different parameters in the SBS process using focused laser beams. The model may help to choose optimal materials, considering their threshold energy and power, phonon lifetime $\tau_{SBS}$, and amplification $g$. For the applied energies and powers of the laser beams the focal length and the length of the cuvette may be optimized. For the given experimental setup the possible reflectivity may be calculated and the intensities of the incident and the reflected light, causing damage and optical breakdown, can be estimated. The necessary minimal coherence length of the laser light can be estimated from the spatial distribution of the second wave in the cuvette.

## ACKNOWLEDGMENTS

Stimulating discussions with A. Kummrow are gratefully acknowledged. D. Schumann and D. Schulze are thanked for their assistance in handling the data. The work was supported by the VOI-Technologiezentrum and the Bundesministerium für Forschung and Technologie.

[1] A. Fisher and I. Abramowitz, ed., Proceedings SPIE 739 (1987).
[2] D. A. Rockwell, IEEE J. Quantum Electron. **24**, 1124 (1988).
[3] M. J. Damzen and M. H. R. Hutchinson, J. Opt. Soc. Am. **152**, 120 (1984).
[4] I. D. Carr and D. C. Hanna, Appl. Phys. B **36**, 83 (1985).
[5] K. V. Gratsianov, A. F. Kornev, V. V. Lyubimov, A. A. Mak, V. G. Pankov, and A. I. Stepanov, Kvant. Elektron. (Moscow) **13**, 5 (1986) [Sov. J. Quantum Electron. **16**, 1 (1986)].
[6] S. Jackel, R. Lalluz, E. Yarkoni, M. Givon, B. Arad, S. Eliezer, and A. Zigler, in *Advances in Laser Science-II*, Proceedings of the Second International Laser Science Conference, edited by W. C. Swalley, M. Lapp, and G. A. Kennedy-Wallace, AIP Conf. Proc. No. 160 (AIP, New York, 1987), p. 130.
[7] V. E. Zuev, P. A. Konyanev, and V. P. Lukin, Bull. Am. Phys. Soc. **32**, 1612 (1987).
[8] N. M. Artemev, S. A. Batishche, K. S. Bagdasarov, A. A. Kuzmuk, N. A. Malevich, V. A. Mostovnikov, V. N. Pismennyi, A. V. Tolstoshev, and E. A. Fedorov, Zh. Prikl. Spektrosk. **47**, 924 (1986) [J. Appl. Spectrosc. (USSR) **47**, 1239 (1987)].
[9] D. A. Rockwell and D. S. Sumida, Proc. SPIE 739, 2 (1987).
[10] P. P. Pashinin and E. I. Shklovsky, J. Opt. Soc. Am. B **5**, 1957 (1988).
[11] A. Jacobs, K. Bowler, M. Farey, D. La Vere, J. Betts, C. G. Koop, C. Glendening, J. Doyle, A. Schnurr, M. Valley, N. K. Moncur, R. Johnson, R. Masters, and D. Ryoo, Proc. SPIE 874, 99 (1988).
[12] N. G. Basov, D. A. Glazkov, V. F. Efimkov, I. G. Zubarev, S. A. Pastukhov, and V. B. Sobolev, IEEE J. Quantum Electron. **25**, 470 (1989).
[13] W. A. Schroeder, M. J. Damzen, and M. H. R. Hutchinson, J. Opt. Soc. Am. B **6**, 171 (1989).
[14] D. R. Hull, R. A. Lamb, and J. R. Digman, Opt. Commun. 72, 104 (1989).
[15] S. Jackel, R. Lalluz, and A. Ludmirsky, Proc. SPIE 1038, 521 (1989).
[16] N. G. Basov, D. A. Glazkov, V. F. Efimkov, I. G. Zubarev, S. A. Pastukhov, and V. B. Sobolev, IEEE J. Quantum Electron. **QE-25**, 470 (1989).
[17] J. Auyeung, D. Fekete, D. M. Pepper, and A. Yariv, IEEE J. Quantum Electron. **QE**-15, 1180 (1979).
[18] P. A. Belanger, A. Hardy, and A. E. Siegman, Appl. Opt. **19**, 602 (1980).
[19] P. A. Belanger, Opt. Eng. **21**, 266 (1982).
[20] G. Giuliani, M.-M. Denariez-Roberge, and P. A. Belanger, Appl. Opt. **21**, 3719 (1982).
[21] D. Pohl, Phys. Lett. **24A**, 239 (1967).
[22] N. N. Ilichev, A. A. Malyutin, and P. P. Pashinin, Kvant. Elektron. (Moscow) **9**, 1803 (1982) [Sov. J. Quantum Electron. **12**, 1161 (1982)].
[23] G. C. Valley and G. J. Dunning, Opt. Lett. **9**, 513 (1984).
[24] P. P. Pashinin, V. S. Sidorin, and E. I. Shklovsky, Kvant. Elektron. (Moscow) **15**, 1755 (1988) [Sov. J. Quantum Electron. **18**, 1092 (1988)].
[25] M. D. Skeldon and R. W. Boyd, IEEE J. Quantum Electron. **QE**-25, 588 (1989).
[26] H. Meng and H. J. Eichler, Opt. Lett. **8**, 569 (1991).
[27] H. J. Eichler, R. Menzel, and D. Schumann, Appl. Opt. (to be published).
[28] M. Valley, G. Lombardi, and R. Aprahamian, J. Opt. Soc. Am. B **3**, 1492 (1986).
[29] D. A. Rockwell and C. R. Giuliano, Opt. Lett. 11, 147 (1986).
[30] R. H. Moyer, SPIE Proc. 1000, 25 (1988).
[31] R. H. Moyer, M. Valley, and M. C. Cimolino, J. Opt. Soc. Am. B **5**, 2473 (1988).
[32] D. T. Hon, Opt. Lett. **12**, 516 (1980).
[33] M. J. Damzen, R. A. Lamb, and G. K. N. Wong (unpublished).
[34] R. A. Mullen, IEEE J. Quantum. Electron. **26**, 1299 (1990).
[35] P. Suni and J. Falk, J. Opt. Soc. Am. B **3**, 1681 (1986).
[36] G. C. Valley, IEEE J. Quantum Electron. **QE-22**, 704 (1986).
[37] P. H. Hu, J. A. Goldstone, and S. S. Ma, J. Opt. Soc. Am. B **6**, 1813 (1989).
[38] Q. Gong, Y. Huang, and J. Yang, Phys. Rev. A **39**, 1227 (1989).
[39] A. Kummrow and H. Meng, Opt. Commun. **83**, 342 (1991).
[40] G. J. Crofts and M. J. Damzen, Opt. Commun. 81, 237 (1991).
[41] M. Maier, Phys. Rev. 166, 113 (1968).
[42] N. F. Andreev, M. A. Dvoretskii, A. A. Leshchev, V. G. Manishin, G. A. Pasmanik, and T. P. Samarina, Kvant. Elektron. (Moscow) **12**, 1402 (1985) [Sov. J. Quantum Electron. **15**, 928 (1985)].
[43] P. Narum, M. D. Skeldon, and R. W. Boyd, IEEE J. Quantum Electron. **QE-22**, 2161 (1986).
[44] G. K. N. Wong and M. J. Damzen, IEEE J. Quantum Electron. **26**, 139 (1990)
[45] Y.-S. Kuo, K. Choi, and J. K. McIver, Opt. Commun. 80, 233 (1991).

[46] L. P. Schelonka and C. M. Clayton, Opt. Lett. **13**, 42 (1988).
[47] J. Munch, R. F. Wuerker, and M. J. LeFebvre, Appl. Opt. **15**, 3099 (1989).
[48] P. Suni and J. Falk, Opt. Lett. **12**, 838 (1987).
[49] J. C. Bellum, T. G. Crow, and E. L. Camp, Opt. Lett. **13**, 36 (1988).
[50] A. F. Vasilév, V. M. Mit'kin, A. N. Shatsev, and V. E. Yashin, Kvant. Elektron. (Moscow) **15**, 771 (1988) [Sov. J. Quantum Electron. **18**, 492 (1988)].
[51] J. J. Ottusch and D. A. Rockwell, Opt. Lett. 16, 371 (1991).
[52] D. Schulze, Diplomathesis, Technical University, Berlin, 1992; H. J. Eichler, R. Menzel, and D. Schulze (unpublished).
[53] M. J. Damzen, M. H. R. Hutchinson, and W. A. Schroeder, IEEE J. Quantum Electron. **QE-19**, 7 (1983).
[54] W. Kaiser and M. Maier, in *Laser Handbook,* edited by F. T. Arecchi and E. O. Schulz (North-Holland, Amsterdam, 1972), pp. 1078–1150.

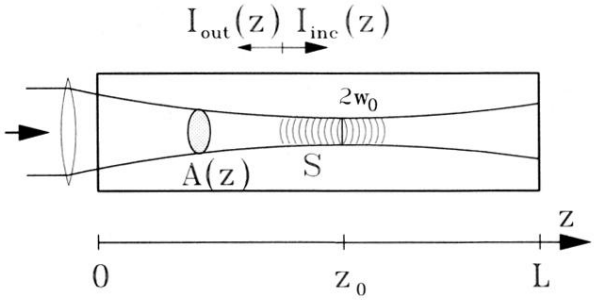


FIG. 1. Intensities $I_{inc}$ and $I_{out}$ and beam area $A$ are functions of the longitudinal coordinate $z$.

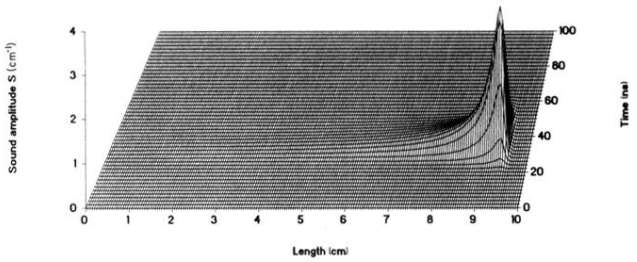


FIG. 15. Distribution of the sound wave in time and space for the standard condition but a phonon lifetime of 17 ns, a gain of 0.0014 cm/MW, and an excitation energy of 25 mJ (compare with Fig. 5).

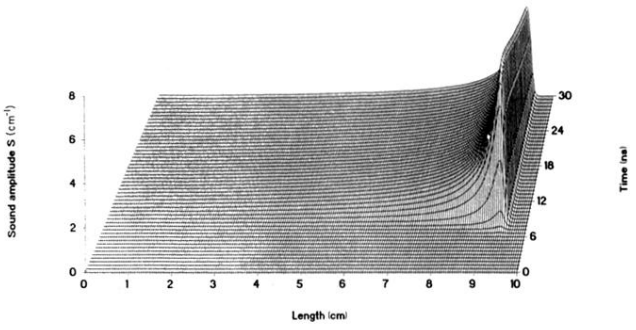


FIG. 18. Distribution of the sound wave in time and space for excitation with 25 mJ, pulse width of 6 ns, and standard conditions otherwise (Compare Fig. 5).

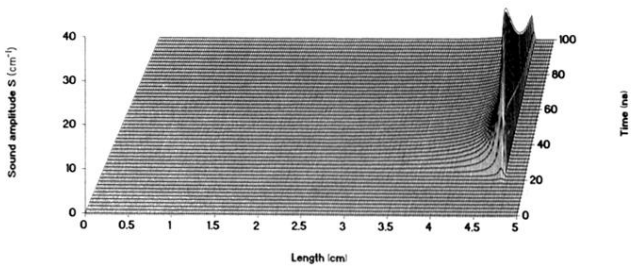


FIG. 19. Distribution of the sound wave in time and space for focusing with an $f = 50$ mm lens and a waist position 47.5 mm behind the cuvette entrance window; standard conditions otherwise.

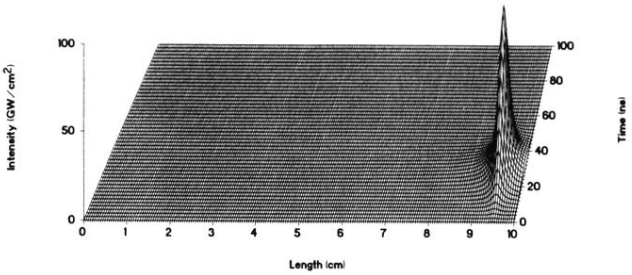


FIG. 2. Spatial and temporal intensity distribution of the incident light pulse of 25 mJ with 20-ns half-width peaking at 30 ns and focused with a 100-mm lens; standard conditions.

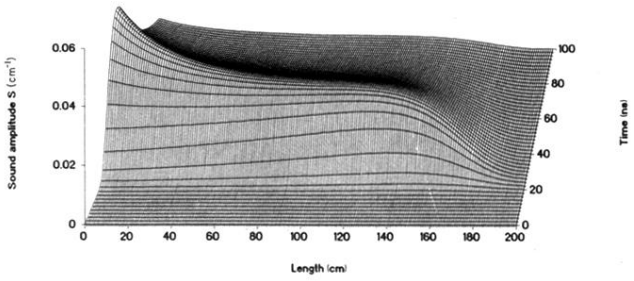


FIG. 20. Distribution of the sound wave in time and space for focusing with an $f = 200$ mm lens and a waist position 190 mm behind the cell entrance window; standard conditions otherwise.

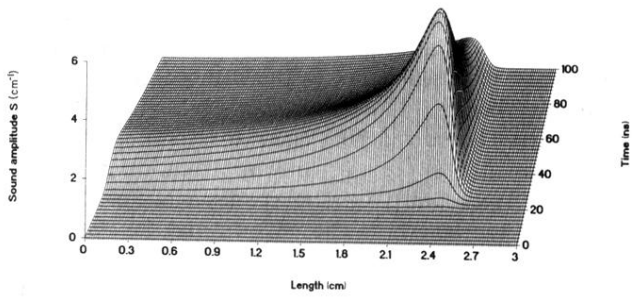


FIG. 22. Distribution of the sound wave in time and space for a waist position 2.5 cm behind the cell entrance window (standard conditions otherwise).

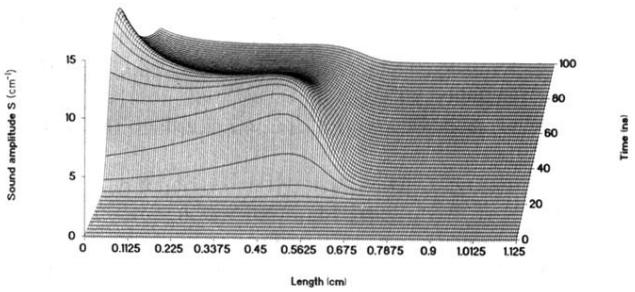


FIG. 23. Distribution of the sound wave in time and space for a waist position 0.625 mm behind the cell entrance window (standard conditions otherwise).

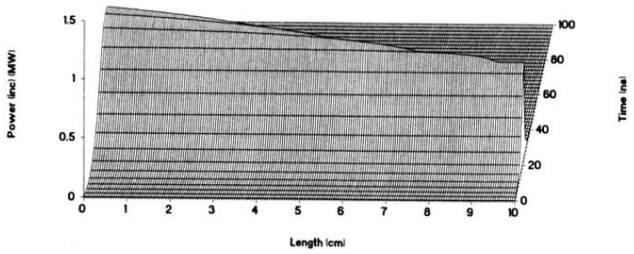


FIG. 3. Power of the incident light pulse; conditions as in Fig. 2.

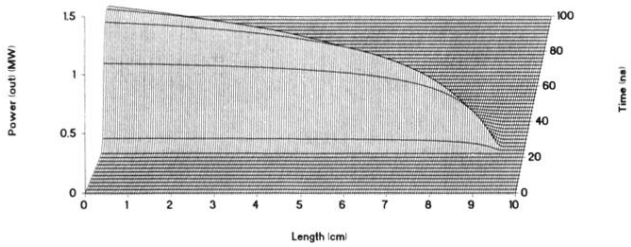


FIG. 4. Power of the reflected light; conditions as in Fig. 2.

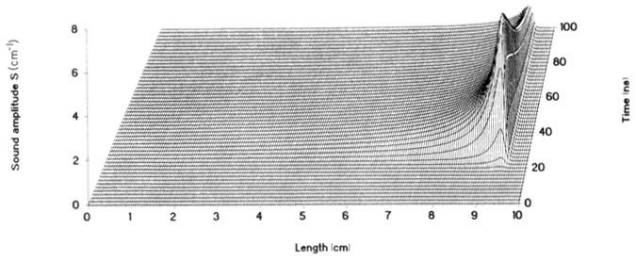


FIG. 5. Amplitude of the sound-wave grating; conditions as in Fig. 2.

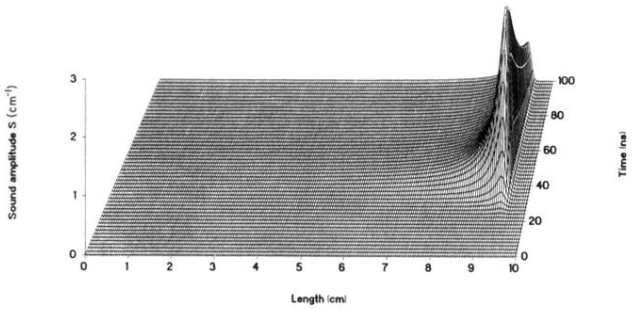


FIG. 8. Distribution of the sound wave in time and space for the excitation of 8 mJ and standard conditions otherwise.

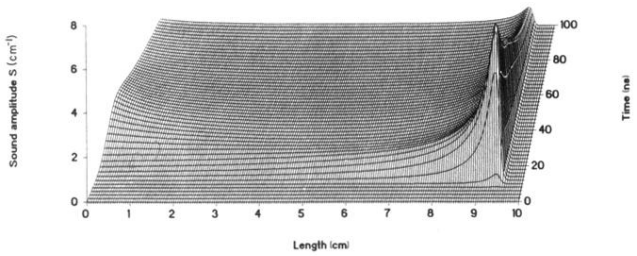


FIG. 9. Distribution of the sound wave in time and space for the excitation of 100 mJ and standard conditions otherwise.